



Neutronics analysis for MSR cell with different fuel salt channel geometries

Shi-He Yu¹ · Ya-Fen Liu¹ · Pu Yang¹ · Rui-Min Ji¹ · Gui-Feng Zhu¹ ·
Bo Zhou¹ · Xu-Zhong Kang^{1,2} · Rui Yan¹ · Yang Zou¹ · Ye Dai¹

Received: 7 September 2020 / Revised: 16 November 2020 / Accepted: 25 November 2020 / Published online: 19 January 2021
© China Science Publishing & Media Ltd. (Science Press), Shanghai Institute of Applied Physics, the Chinese Academy of Sciences, Chinese Nuclear Society 2021

Abstract The neutronic properties of molten salt reactors (MSRs) differ from those of traditional solid fuel reactors owing to their nuclear fuel particularity. Based on the Monte-Carlo N particle transport code, the effects of the size and shape of the fuel salt channel on the neutron physics of an MSR cell are investigated systematically in this study. The results show that the infinite multiplication factor (k_{∞}) first increases and then decreases with the change in the graphite cell size under certain fuel volume fraction (FVF) conditions. For the same FVF and average chord length, when the average chord length is relatively small, the k_{∞} values for different fuel salt channel shapes agree well. When the average chord length is relatively large, the k_{∞} values for different fuel salt channel shapes differ significantly. In addition, some examples of practical applications of this study are presented, including cell selection for the core and thermal expansion displacement analysis of the cell.

Keywords Molten salt reactor · Fuel salt channel · Cell geometry · Neutronics

1 Introduction

As one of the six Gen-IV reactor types, the molten salt reactor (MSR) was first investigated in the 1950s to as a method to provide a compact high-temperature power plant for nuclear powered aircraft [1]. Subsequently, an aircraft reactor experiment was constructed at the Oak Ridge National Library, USA, in which the nuclear feasibility of operating a molten salt-fueled reactor at high temperature was demonstrated [2]. After discovering the high potential of the MSR for achieving low electric-power-generating costs in central power plants, a molten salt reactor experiment (MSRE) was performed successfully [3]. In addition, a critical experiment device (hereinafter the device) was established at the Shanghai Institute of Applied Physics (originally known as the Shanghai Institute of Nuclear Research), China, in the 1970s. Its main purpose was to reveal the physics of MSRs and thorium–uranium cycles. Although studies regarding the MSR has not been interrupted, an actual reactor has not been built [4–6].

After rediscovering that MSRs offer unique advantages in terms of inherent safety, economy, sustainable development of nuclear fuel, and nonproliferation, studies regarding MSRs has re-emerged and progressed since the 21st century [7–9]. To satisfy national strategic requirements in the field of nuclear energy, the Chinese Academy of Sciences launched a strategic and pioneering science and technology project known as “Future Advanced Fission Energy-Thorium-based Molten Salt Reactor Nuclear Energy System” in 2011. Subsequently, the Thorium Molten Salt Reactor (TMSR) Center was established; it is dedicated to the research and development of Gen-IV advanced fission reactor nuclear energy systems for achieving strategic goals such as diversifying nuclear fuel,

This work was supported by the Chinese TMSR Strategic Pioneer Science and Technology Project (No.XDA02010000), the Frontier Science Key Program of Chinese Academy of Sciences (No.QYZDY-SSW-JSC016), and the Shanghai Sailing Program (No. Y931021031).

✉ Ya-Fen Liu
liuyafen@sinap.ac.cn

¹ Shanghai Institute of Applied Physics, Chinese Academy of Sciences, Shanghai 201800, China

² University of Chinese Academy of Sciences, Beijing 100049, China

preventing nuclear proliferation, and minimizing nuclear waste. The preliminary target of the project was to build a 2 MW thorium-based MSR [10, 11].

MSRs are a type of thermal neutron reactor that involves a molten salt mixture fuel cycle and is moderated by graphite to produce fission energy. Molten salt mixture fuel can be the fluoride of uranium, thorium, zirconium, etc., and is used as both a nuclear fuel and heat carrier under a high-temperature liquid without requiring solid fuel elements [12]. In general, the physical characteristics of the core have been investigated by varying the volume ratio between the moderator and the nuclear fuel in thermal reactors, such as pressurized water reactors [13, 14]. For an MSR, its lattice cell is a component of the traditional reactor. The cells are typically columnar graphite blocks, and the side length increases with the core size. For example, the side length of the regular quadrilateral graphite lattice cell used in the MSRE was 5 cm, whereas the side length of the hexagonal graphite lattice cell of the molten salt breeder reactor (MSBR) was 15 cm [15–18]. Despite two graphite cells having the same geometric shape and the same graphite-to-fuel salt volume ratio, the different sizes of the cells will change the neutron physical properties. The geometry of liquid nuclear fuel in MSRs is flexible, allowing MSRs to have fuel cells of various shapes. In addition, because the coefficient of thermal expansion between graphite and alloy differ significantly, the change in the core geometry owing to high temperature should not only be attributed to the thermal expansion of each component, but also the graphite cell displacement. New fuel salt channels can be formed between the graphite cells after the latter are displaced, and their geometric shapes differ from that of the original fuel salt channel [19]. Therefore, the neutron physical properties of different graphite cell sizes and fuel salt channel shapes must be investigated.

Based on the Monte–Carlo N particle transport code (MCNP), several types of graphite cell models of fuel salt channels with different sizes and geometric shapes are presented herein [20, 21]. In this study, the effects of the size and geometric shapes of the fuel salt channel on the infinite multiplication factor k_∞ and neutron energy spectrum of the cell were investigated. In addition, the variation law of k_∞ with the average chord length of the fuel salt channel under different fuel salt volume ratios and heavy metal molar ratios was calculated and analyzed. Finally, some practical application examples of this study are presented, and they can be used as a reference for the design of MSRs.

2 Models and parameters

MSRs are manufactured in many forms; however, liquid fuel salts typically flow through cores made of graphite with a critical geometry. Heat is produced by the fission of the fuel salt and then dissipated by the flowing fuel salt. Fuel is concentrated into blocks in an inhomogeneous reactor, such as cylinders, circles, spheres, and sheets (planks), which are placed in a moderator of a specific geometric form to form the core of the lattice structure. The elementary units that compose a lattice structure are generally known as cells [22]. The fuel salt channel in an MSR corresponds to the fuel block in the traditional reactor. For this study, only the variation trend of the k_∞ of the cell was considered in this study. Subsequently, the neutron physics law of the corresponding cell type was obtained via k_∞ value analysis. Therefore, the entire core need not be modeled. k_∞ is related to the size and shape of the fuel salt channel, and the effects of the size and shape of the fuel salt channel on k_∞ can be constrained by the average chord length of the fuel salt channel L . As shown in Formula (1), the average chord length of the fuel salt channel is defined as four times the volume of the fuel salt channel V divided by the surface area of the fuel salt channel S [22].

$$L = \frac{4V}{S} \quad (1)$$

As shown in Fig. 1, several basic fuel salt channel models with different shapes were established using MCNP6 for comparative analysis in this study, including

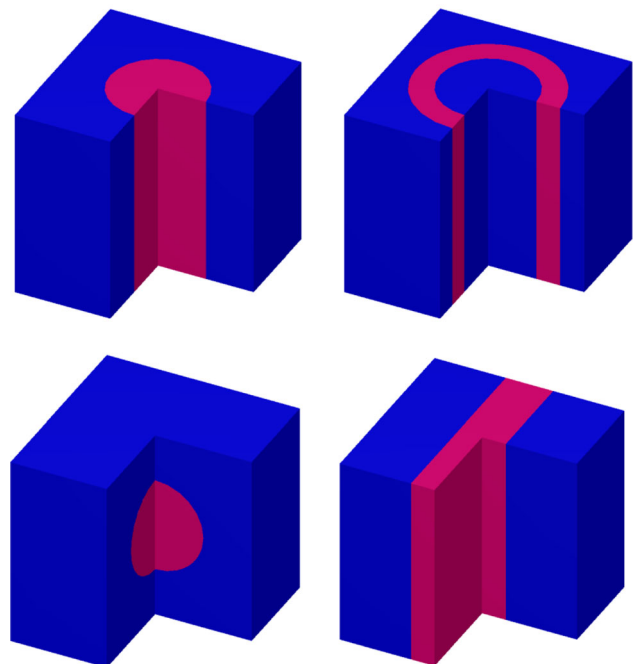


Fig. 1 (Color online) Schematic diagrams of computational models

cylindrical, annular, spherical, and flaky [20, 21]. The central region of each cell in Fig. 1 represents the fuel salt and the surrounding region represents graphite. Typically, a cylindrical shape is selected for the fuel channel of the MSR, e.g., the MSBR for breeding purposes. The well-known fuel salt channel of the MSRE is the runway type and can be regarded as a combination of cylinders and flakes. After the displacement of the graphite cell, the new fuel salt channel formed between cells is generally flake shaped. Circular and spherical fuel salt channels were selected for result comparison. It is noteworthy that the fuel salt can flow up and down by gouging out a channel above and below the sphere. The cell is segmented into a fuel salt zone and a graphite moderator zone. For example, in the cylindrical fuel salt channel model, the fuel salt zone is the cylindrical zone, and the graphite moderator zone is located outside the cylinder. Key parameters such as the fuel salt composition and density used by the cell are shown in Table 1. The fuel salt composition is consistent with the MSRE; therefore, the trend of density change with temperature can be obtained from MSRE technical report data [3]. The density of the fuel salt was 2.34 g/cm^3 at $550 \text{ }^\circ\text{C}$. T220-graphite with a density of 1.86 g/cm^3 at room temperature and a linear thermal expansion coefficient of $3.49 \times 10^{-6}/^\circ\text{C}$ at room temperature to $550 \text{ }^\circ\text{C}$ were used in this study [3]. The average temperature of the cell was $550 \text{ }^\circ\text{C}$, which was used in the calculation and analysis of this study. Nuclear data library ENDF/B-VII.0 was used for the calculation performed in this study, and its applicability and advantages to MSRs have been verified by Liu Yafen et al. in 2018 [5, 23]. For result comparison, all the calculations were performed under the same condition, i.e., the number of source neutrons selected for each cycle were 100,000, with 1050 active cycles and 50 abandoned cycles, resulting in a standard deviation of approximately 0.00005.

Even if the fuel salt fraction and the fuel volume fraction (*FVF*) are the same, the k_∞ of the cell is still related to the cell arrangement, an aspect not considered herein. When changing the average chord length, only a relatively convenient method was adopted in this study, and the

difference in k_∞ caused by other methods was not considered. The method is described in detail as follows: the average chord lengths of the cylindrical and spherical fuel salt channels were changed by changing the channel size. The average chord length of the circular fuel salt channel was changed by changing the outer diameter of the circular fuel salt channel. In addition, the average chord length of the flaky fuel salt channel was changed by changing the thickness of the flaky fuel salt channel. The *FVF* of the cell was maintained constant when the average chord length was changed in the cases above. First, the effects of the size and geometric shapes of the fuel salt channel on k_∞ and the neutron energy spectrum of the cell was investigated. Subsequently, the variation law of k_∞ with the average chord length of the fuel salt channel under different *FVF* values and heavy metal molar ratios was calculated and analyzed. Finally, some practical application examples of this study are presented.

3 Results and discussion

3.1 Effect of fuel salt channel geometry

As described in the previous section, the fuel salt channel geometric shapes considered in this section include cylindrical, circular, spherical, and flaky. The effects of different geometric shapes on k_∞ and the neutron energy spectrum of the cell are analyzed in this section. In addition, the physical causes of those effects were analyzed along with the calculation results. Table 2 shows the graphite cell side length of the fuel salt channel with different geometric shapes under the same average chord length. The data in the table are important input parameters for the subsequent calculation in this study. It can be assumed that under the same average chord length, the graphite cell side length of the fuel salt channel with different shapes differs significantly.

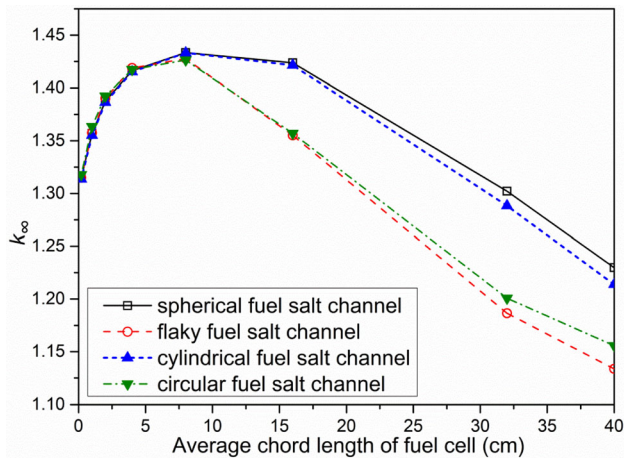
Figure 2 shows the variation of k_∞ with the average chord length of fuel salt channel under different fuel salt

Table 1 Parameters of graphite cell model

Parameter	Value
Fuel salt composition (mole)	65.39%LiF-25.34%BeF ₂ -4.72%ZrF ₄ -1.55%UF ₄
Fuel salt density at $550 \text{ }^\circ\text{C}$ (g/cm^3)	2.34
²³⁵ U enrichment (%)	17
Graphite density at $550 \text{ }^\circ\text{C}$ (g/cm^3)	1.86
Linear thermal expansion coefficient of graphite at room temperature to $550 \text{ }^\circ\text{C}$ ($^\circ\text{C}^{-1}$)	3.49×10^{-6}
Linear thermal expansion coefficient of Hastelloy-N at room temperature to $550 \text{ }^\circ\text{C}$ ($^\circ\text{C}^{-1}$)	13.40×10^{-6}
Fuel salt temperature ($^\circ\text{C}$)	550

Table 2 Side length of cell with different fuel salt channel geometric shapes

L (cm)	1.00	2.00	4.00	8.00	16.00	32.00	40.00
Side length of cell with cylindrical fuel channel (cm)	2.29	4.58	9.15	18.31	36.60	73.20	91.02
Side length of cell with flaky fuel channel (cm)	3.83	7.67	15.33	30.67	61.33	122.67	153.33
Side length of cell with spherical fuel channel (cm)	2.28	4.55	9.11	18.20	36.41	72.80	91.00
Side length of cell with circular fuel channel (cm)	3.96	7.92	15.85	31.70	63.40	126.79	158.49

**Fig. 2** (Color online) k_∞ at different chord lengths for different fuel salt channel shapes

channel geometric shapes. As shown in the figure, when the average chord length was relatively small ($L < 7.5$ cm), the k_∞ of the fuel salt channel with different geometric shapes agreed well. This was because when the same L value was less than 7.5 cm, the energy spectrum of the fuel region under different geometric shapes was similar. As the average chord length increased to 7.5 cm, the difference in k_∞ of the fuel salt channel with different geometric shapes began to be significant. In addition, in the relatively large range (7.5–40 cm) of the average chord length, the k_∞ of the cylindrical and spherical fuel salt channel was greater than that of the flaky or circular fuel salt channel. By contrast, the k_∞ of the flaky and circular fuel salt channels were similar. Meanwhile, the k_∞ of the cylindrical fuel salt channel was similar to that of the spherical fuel salt channel.

Figure 3 shows the normalized neutron flux distributions of the cell (left) and fuel salt zone (right) with different geometric shapes. The FVF of each cell was 15%, and the average chord length was set to 16 cm. As shown from the figure, the neutron spectra of the cells with circular and flaky fuel salt channel shapes were consistent. In addition, the neutron spectrum of the cell with a cylindrical fuel salt channel was similar to that of a cell with a spherical fuel salt channel. As shown from the normalized neutron flux

distribution in the cell (the left of Fig. 3), the neutron spectra of the cells with flaky and circular fuel salt channels were relatively thermal, and the thermal neutron utilization factor was small. Furthermore, the normalized neutron flux distribution in the fuel salt (the right of Fig. 3) indicates that the neutron spectra of the flaky and circular fuel salt channels were relatively hard, and the neutron share in the resonance absorption region increased correspondingly. Therefore, in the interval with a relatively large average chord length, the variation in k_∞ appeared as shown in Fig. 2.

Through the calculation and analysis above, it was discovered that although the FVF and fuel concentration (FC) of the cell were the same, the geometric shapes of the fuel and salt channels differed. This affected the neutron spectrum significantly, resulting in a significant discrepancy in k_∞ . The average chord length had a certain constraint on k_∞ . When the average chord length was relatively small (less than 10 cm), the k_∞ of the fuel salt channel with different geometric shapes agreed well. In the interval with a relatively large average chord length (greater than 10 cm), the k_∞ variation trends of the fuel salt channel with different geometric shapes were the same, but the specific k_∞ values differed significantly. The next section provides the detailed reasons for these significant k_∞ differences.

3.2 Effect of fuel salt channel size

A graphite cell with a circular fuel salt channel was selected for calculation and analysis in this study. Based on the material composition of the cell and an FVF value of 15%, the cell size was changed to calculate the variation in k_∞ . The variation curve of this value is shown in Table 3, and the reason for the change based on the four factors and the neutron energy spectrum of the cell is emphasized in this section. The method to calculate the four factors has been provided by Sun Jianyou et al. in 2014 [24, 25]. The results of these factors are also listed in Table 3, where ϵ is the fast neutron multiplication factor, p is the probability of escape resonance absorption, η is the effective number of fission neutrons, and f is the thermal utilization factor.

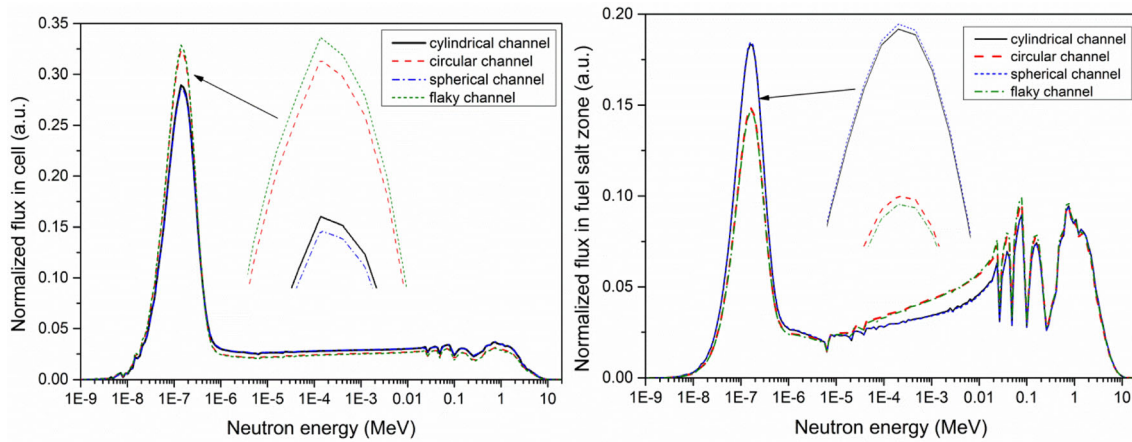


Fig. 3 (Color online) Neutron spectrum of cell (left) and fuel salt zone (right) for different fuel salt channel shape with $L = 16$ cm

Table 3 Variations of four factors with radius of fuel salt channel

Fuel salt channel radius (cm)	0.5	1.0	2.0	4.0	8.0	12.0	16.0	20.0
ϵ	1.08291	1.08107	1.07896	1.07611	1.07600	1.10451	1.13528	1.18708
p	0.78633	0.80635	0.82658	0.84465	0.85663	0.82149	0.78896	0.73737
η	1.64413	1.64401	1.64504	1.64313	1.64264	1.64247	1.64239	1.64214
f	0.96802	0.96729	0.96537	0.95946	0.93877	0.90875	0.87553	0.84484
k_∞ calculated based on four-factor formula	1.35525	1.38625	1.41633	1.43296	1.42136	1.35685	1.28797	1.21437
k_∞ calculated via MCNP6	1.35513	1.38642	1.41524	1.43321	1.42142	1.39675	1.28830	1.21383

As shown in Table 3, as the fuel salt channel radius increased, the k_∞ value first increased and then decreased. The variation of the four factors is summarized as follows:

- ϵ first decreased and then increased;
- p first increased and then decreased;
- η was unaffected by the change in the fuel salt channel radius;
- f decreased as the fuel salt channel radius increased.

The results indicate that the variation in k_∞ was primarily caused by the escape resonance absorption probability p and thermal neutron utilization coefficient f . Although the fast neutron multiplication factor ϵ affected k_∞ , the amplitude of its variation was much smaller than that of the escape resonance absorption probability.

Figure 4 shows the normalized neutron flux distributions in the cell (left) and fuel salt zones (right) with different fuel salt channel radii, where R is the radius of the fuel salt channel. With the increase in the fuel salt channel radius, the neutron spectrum of the cell tended to be thermal. This was because as the fuel salt channel radius as well as the distance between the channels increased, the graphite area expanded, increasing the probability of the fast neutron in the graphite to decelerate to less than the resonance energy. In other words, the share of thermal neutron flux in graphite

increased, resulting in a decrease in the thermal neutron utilization of the cell. Resonance neutrons were primarily produced in graphite moderators and then incident on the fuel salts. Because of the large resonance absorption cross-section of the nuclei in the fuel, the resonance neutrons were first absorbed by the nuclei on the surface of the fuel salt channel and served as a shield to the nuclei inside the fuel salt channel. ΔR denotes the resonant absorption surface of the fuel salt channel, and R is the radius of the fuel salt channel. An increase in R will not cause a change in ΔR , and the area where neutrons are not absorbed by resonance will increase. In other words, the spatial self-screen effect becomes more prominent, whereas the resonance absorption decreases and the probability of escaping resonance absorption increases.

However, as shown from the right side of Fig. 4, the neutron flux distribution of the fuel salt zone shows that the spectrum became harder as the radius of the fuel salt channel increased. In particular, the spectrum exhibited a clear hardening trend when the radius of the fuel salt channel exceeded 8 cm. This was primarily because the fuel salt contained moderated materials, such as lithium and beryllium. When the radius of the fuel salt channel increased, the probability of neutron reaction in the fuel salt increased; consequently, the probability of neutrons

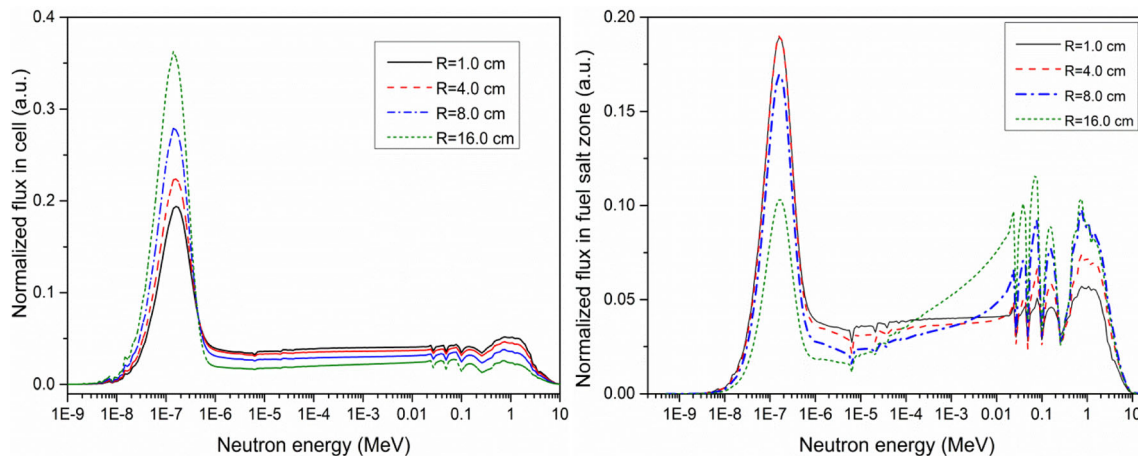


Fig. 4 (Color online) Neutron spectrum of cell (left) and fuel salt zone (right) under different fuel salt channel radii

decelerating to the resonance region in the fuel salt increased. In other words, as the resonance absorption of the neutron increased, the probability of escaping from the resonance absorption decreased.

Based on the analysis above, when the *FVF* of the cell with a cylindrical fuel salt channel was set to 15%, the probability of escaping from the resonance absorption first increased and then decreased with the increase in the fuel salt channel radius. The thermal neutron utilization coefficient always decreased as the channel radius increased. Therefore, the overall effect was that as the fuel salt channel radius increased, k_{∞} first increased and then decreased. It is noteworthy that the fuel salt can decelerate neutrons. Therefore, resonance neutrons were also produced in the fuel salt region, thereby affecting the resonance absorption of the cell.

3.3 Effects of *FVF* and *FC*

The moderator-to-fuel volume ratio and the composition of the nuclear fuel directly affected the physical properties of the core. The variation law of the k_{∞} value of the cell was obtained based on the fuel salt volume ratio and fuel salt heavy metal molar ratio. This section focuses on the analysis of the variation law of k_{∞} with the average chord length under different *FVFs* and *FCs*. The *FVF* value of the cell was changed by adjusting the size of the graphite portion, whereas the size of the fuel salt channel remained unchanged. The *FVFs* were set to 5%, 15%, and 30%. The effect of the *FC* on k_{∞} was also investigated, and the *FCs* were set to 1.55%, 4%, and 8%.

Figure 5 shows the k_{∞} variation of a cell with a cylindrical fuel salt channel under different *FVFs* and *FCs* with changes in the fuel salt channel radius. Although k_{∞} was significantly affected by the *FVF*, under different *FVFs*, it first increased and then decreased with the change in the

fuel salt channel radius. In the case of *FVF* = 5%, when the fuel channel radius was less than 1.5 cm, k_{∞} increased with the fuel channel radius; k_{∞} decreased as the channel radius increased when the fuel channel radius was larger than 1.5 cm. In other words, k_{∞} was maximized at a fuel channel radius of 1.5 cm. Furthermore, k_{∞} was maximized at fuel channel radii of 4.5 and 8 cm in cases where *FVF* = 15% and 30%, respectively. When *FC* = 1.55% and the fuel channel radius was less than 4 cm, k_{∞} increased with the fuel channel radius. Furthermore, k_{∞} decreased as the channel radius increased when the fuel channel radius exceeded 4 cm. Additionally, k_{∞} was maximized at a fuel channel radius of 7.5 cm when *FC* = 4% and 8%. The k_{∞} variation trend of the fuel channel radius remained unchanged, and only the radius of the fuel salt channel corresponding to the maximum k_{∞} value changed. This was primarily due to the different degrees of neutron decelerating under different *FVFs* and *FCs*, resulting in different neutron energy spectra.

Figures 6 and 7 show the variation in k_{∞} of the fuel salt channel with the average chord length of the fuel salt channel under different *FVFs* and *FCs*, respectively. PZ, Q, YZ, and YH represent the flaky, spherical, cylindrical, and circular fuel salt channels, respectively. It was observed that the variation law of k_{∞} with the average chord length was consistent under different *FCs* for the four fuel salt channels with different geometric shapes. In addition, the variation law of k_{∞} with the average chord length was consistent under different *FVFs* except for the case of a circular fuel salt channel with an *FVF* of 5%. Figure 8 shows the normalized neutron spectrum in the cell of the circular fuel salt channel. In the region where *FVF* was low and the average chord length was large, owing to the increase in the fast neutron multiplication coefficient, the spectrum became harder with the increase in the average chord length. The thermal neutron utilization coefficient

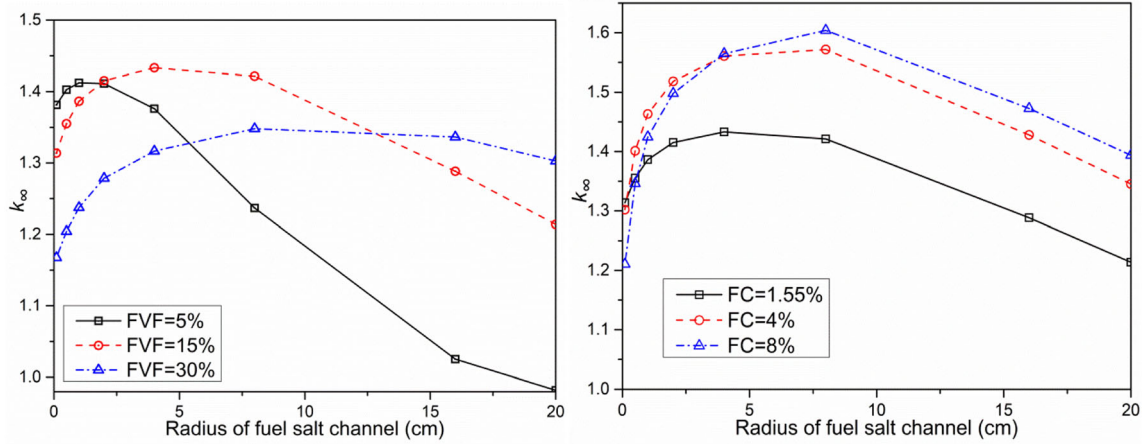


Fig. 5 (Color online) Effect of fuel salt channel radius on k_{∞} for different FVFs (left) and FCs (right)

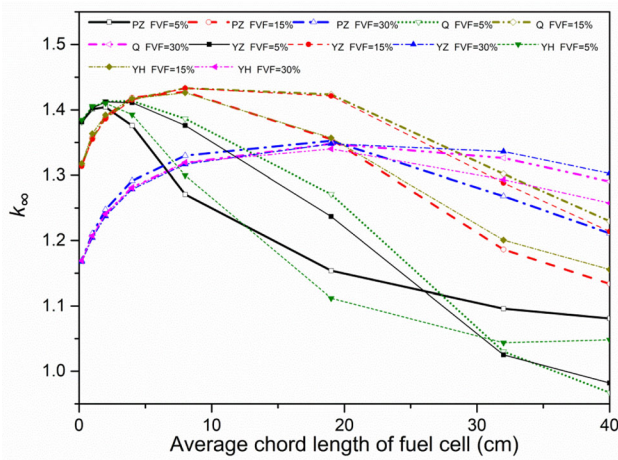


Fig. 6 (Color online) Effect of average chord length on k_{∞} for different FVFs

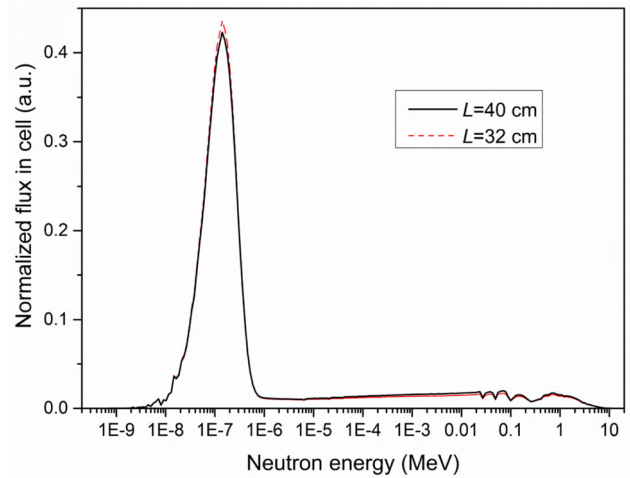


Fig. 8 Normalized neutron spectrum of circular cell

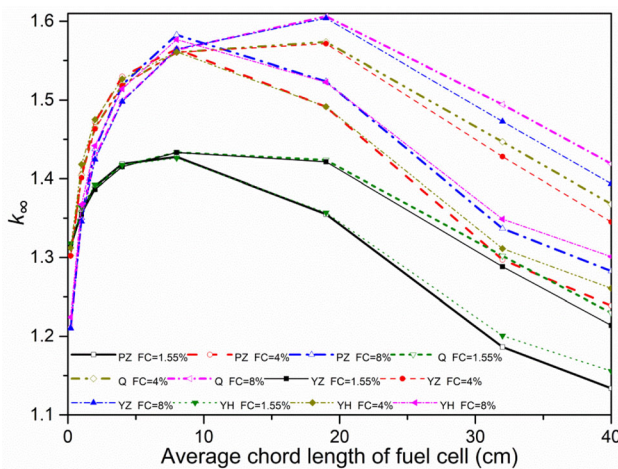


Fig. 7 (Color online) Effect of average chord length on k_{∞} for different FCs

increased correspondingly. Therefore, k_{∞} tended to increase again.

Similarly, for the fuel salt channel cells with the same *FVF* and *FC*, the k_{∞} of the fuel salt channels with different geometric shapes agreed well in the interval with an average chord length of less than 10 cm. The k_{∞} of the fuel salt channel with different geometric shapes differed significantly in the range of the average chord length greater than 10 cm. Moreover, the variation laws of k_{∞} with the average chord length of the cells with flaky and circular fuel salt channels were similar, whereas those of the cells with cylindrical and spherical fuel salt channels were similar. In summary, although the FVFs and FCs differed, the variation law of the k_{∞} of the cell with the average chord length was universal.

4 Application examples

In the research and design of actual MSRs, the appropriate size and shape of the grid element must be selected. MSR cores can be large or small, and large graphite cells can be used for large cores to enhance the strength of the cell mechanical structure. Additionally, the characteristics of the MSR, namely its high-temperature state and the flow properties of the fuel salt, determine the geometric diversity of the fuel salt channel in the core. Therefore, investigations regarding the effects of different flow passage geometries on neutron physics can provide a reference for the selection of graphite cells.

4.1 Cell selection

The fuel assembly in the molten salt core is the graphite cell in the core. According to the calculation data in Table 3, when the *FVF* was fixed, i.e., for the same fuel salt load of the core, a maximum k_{∞} value occurred with the change in the graphite cell size. Therefore, for a specific *FVF*, the graphite cell size can be reasonably selected only if k_{∞} is considered in the optimal design of the cell.

As shown in Fig. 2, the fuel salt channel with different geometric shapes had the same k_{∞} for the same *FVF* when the average chord length was relatively small. As shown in Table 2, for the same average chord length, the graphite cell side length of the fuel salt channel with different geometric shapes varied significantly. Therefore, for the same k_{∞} , the lengths of the graphite cells with flaky and circular fuel salt channels were much larger than those with cylinder and spherical fuel salt channels. The flaky or circular fuel salt channels can be used when larger graphite cells are required.

4.2 Effect of expansion displacement on cell

In an MSR, graphite is located on an alloy support plate. A significant difference exists in the expansion coefficient between the graphite and alloy, rendering the spacing between the graphite gate elements more conspicuous at high temperatures; hence, the graphite cell is displaced. Owing to the fluidity of the fuel salt, the gap between the graphite cells is filled with the fuel salt after the graphite cell displacement. Therefore, after the expansion and displacement of the graphite cells, not only did the *FVF* change, but also a new fuel salt channel was formed between the cells, and the geometric shape differed from that the original fuel salt channel. These changes will affect the physical properties of the core.

The reference fuel salt channel was assumed to be cylindrical and its *FVF* value 15%. The second row in

Table 4 lists the k_{∞} values of this reference cell for different chord lengths. As the temperature increased from 550 to 700 °C (accident temperature), the graphite cells shifted owing to the difference in thermal expansion coefficient between graphite and Hastelloy-N. Areas that enlarged due to differences in the coefficient of thermal expansion were filled with the fuel salt. Consequently, the *FVF* increased from 15 to 15.4% and a flaky new fuel salt channel appeared around the graphite cell. Line 5 in Table 4 shows the deviations between the k_{∞} values of the cell after displacement and the corresponding reference k_{∞} values. To distinguish the effect of the *FVF* on the neutron physical properties of the cell, the fuel salt channel radius was fixed, and the side length of the graphite gate element was artificially reduced to obtain k_{∞} values by increasing the *FVF* to 15.4%. Line 4 shows the differences between these k_{∞} values and those of the corresponding cells after displacement. In summary, the difference shown in the third row in Table 4 reflects the effect of *FVF* increase on k_{∞} . The difference in line 4 reflects the effects of different cell geometries (cylindrical and flaky) of a new fuel salt channel on k_{∞} .

As shown by the comparison results in Table 4, the *FVF* changed and formed new fuel salt channels owing to the expansion displacement of the graphite cell, thereby affecting k_{∞} . In addition, the effects of the two above-mentioned factors on the k_{∞} of the cell changed under different cell sizes. Therefore, the effect of material expansion displacement should be considered in the core design. Alternatively, the cell can be bound to prevent the cell from moving with the support plate.

5 Conclusion

Several graphite cell models of fuel salt channels with different sizes and shapes were established in this study, and the effects of the size and shape of the fuel salt channel on k_{∞} and the neutron energy spectrum of the cell were investigated. Additionally, the variation laws of k_{∞} with the average chord length of the fuel salt channel under different fuel salt volume ratios and heavy metal molar ratios were calculated and analyzed. Some practical application examples of this study were illustrated toward the end. The results indicated that, owing to variations in the size and shape of the cell, the types and times of nuclear reactions between neutrons and the material in the cell from neutron generation to absorption changed, resulting in a change in the physical properties of the cell. The main conclusions were as follows:

- (1) Within a certain range of *FVF* and *FC*, k_{∞} first increased and then decreased as the average chord

Table 4 Effects of different factors on k_{∞}

L (cm)	1.00	2.00	4.00	8.00	16.00	32.00	40.00
k_{∞}	1.35513	1.38642	1.41524	1.43321	1.42142	1.28830	1.21383
Effect of increasing FVF on k_{∞}	− 0.00376	− 0.00392	− 0.00279	− 0.00193	0.00001	0.00443	0.00494
Effect of different geometries on k_{∞}	− 0.00354	− 0.00478	− 0.00707	− 0.00769	− 0.00397	0.02587	0.04636
Effect of expansion displacement on k_{∞}	− 0.00730	− 0.00870	− 0.00986	− 0.00962	− 0.00396	0.03030	0.05130

length increased. In addition, the difference in k_{∞} of the fuel salt channel with different geometric shapes increased with the average chord length.

- (2) The neutron spectrum in the cell became thermal, and the spectrum in the fuel salt region became hard as the average chord length increased. The neutron spectrum of the flaky fuel salt channel was similar to that of the circular fuel salt channel. Meanwhile, the neutron spectrum of the cylindrical fuel salt channel was similar to that of the spherical fuel salt channel. Therefore, the variation laws of k_{∞} with the average chord length of the cells with flaky and circular fuel salt channels were similar, whereas those of the cells with cylindrical and spherical fuel salt channels were similar.
- (3) For the fuel salt channel cells with the same *FVF* and *FC*, the k_{∞} of the fuel salt channels with different geometric shapes agreed well in the interval with an average chord length less than 10. The k_{∞} of the fuel salt channel with different geometric shapes differed significantly when the average chord length was greater than 10 cm.
- (4) The variation law of the k_{∞} of the cell with the average chord length was universal and independent of the *FVF* and *FC*.

The results of this study demonstrated the basic physical law of different geometrical fuel channel cells for MSRs and can provide a reference for selection, to some extent. The section toward the end of this article presents some application examples of this study. For the future, relevant studies regarding the hydraulic and thermal properties of cells with different shapes of fuel channels, e.g., the temperature distribution of the cell and the flow field distribution of the fuel channel, will be performed. Furthermore, the safety performance of the cores composed of these cells will be verified. Ultimately, the knowledge of neutron physics and thermal–hydraulic characteristics can provide a good foundation for the core selection optimization of MSRs. The results of this study provide a basis for future engineering applications.

Author contributions All authors contributed to the study conception and design. Material preparation, data collection, and analysis were performed by Shi-He Yu, Ya-Fen Liu, and Pu Yang. The first draft of the manuscript was written by Ya-Fen Liu, and all authors commented on previous versions of the manuscript. All authors read and approved the final manuscript.

References

1. R.C. Briant, A.M. Weinberg, Molten fluorides as power reactor fuel. *Nucl. Sci. Eng.* **2**, 797–803 (1957). <https://doi.org/10.13182/NSE57-A35494>
2. E.S. Bettis, R.W. Schroeder, G.A. Cristy et al., The aircraft reactor experiment—design and construction. *Nucl. Sci. Eng.* **2**, 804–825 (1957). <https://doi.org/10.13182/NSE57-A35495>
3. P.N. Haubenreich, J.R. Engel, Experience with the Molten-Salt Reactor experiment. *Nucl. Appl. Technol.* **8**, 118–136 (1970). <https://doi.org/10.13182/NT8-2-118>
4. S. Ling, Zero Power Experiment Device in Shanghai Institute of Nuclear Research. *Chin. J. Nucl. Sci. Eng.* **2**, 23–24 (1984). (in Chinese)
5. Y. Liu, R. Yan, Y. Zou et al., Criticality properties and control rod worth of the critical experiment device for MSR research. *Nucl. Technol.* **204**, 203–212 (2018). <https://doi.org/10.1080/00295450.2018.1474703>
6. Y. Liu, R. Yan, Y. Zou et al., Neutron flux distribution and conversion ratio of Critical Experiment Device for molten salt reactor research. *Ann. Nucl. Energy* **133**, 707–717 (2019). <https://doi.org/10.1016/j.anucene.2019.07.018>
7. USDOE, A Technology Roadmap for Generation IV Nuclear Energy Systems. *J. Philosophical Rev.* **66**, 239–241(2002). GIF-002-00
8. I. L. Pioro, Handbook of Generation IV Nuclear Reactors. M. Elsevier Inc, (2014). <https://doi.org/10.1016/C2014-0-01699-1>
9. M. Brovchenko, D. Heuer, E. Lucotte et al., Design-related studies for the preliminary safety assessment of the Molten Salt Fast Reactor. *Nucl. Sci. Eng.* **175**, 329–339 (2012). <https://doi.org/10.13182/NSE12-70>
10. M. Jiang, H. Xu, Z. Dai, The Future of advanced nuclear fission energy-TMSR nuclear energy systems. *Bull. Chin. Acad. Sci.* **27**, 366–374 (2012). (in Chinese)
11. X. Cai, Z. Dai, H. Xu, Thorium molten salt reactor nuclear energy system. *Physics* **45**, 578–590 (2016). <https://doi.org/10.7693/wl20160904>. (in Chinese)
12. Q. Ye, X. Li, Z. Yu, et al., China electrical engineering canon sixth volume nuclear power generation engineering. Beijing: China Electric Power Press, 1142–1144 (2009). (in Chinese)
13. S. Yu, X. Cao, B. Lan, Analysis of moderator temperature coefficient with neutron spectrum for pressurized water reactors. *Atomic Energy Sci. Technol.* **47**, 1594–1598 (2013). (in Chinese)

14. J.S. Kim, Y.S. Jeon, S.D. Park et al., Analysis of high burnup pressurized water reactor fuel using uranium, plutonium, neodymium, and cesium isotope correlations with burnup. *Nucl. Eng. Technol.* **47**, 924–933 (2015). <https://doi.org/10.1016/j.net.2015.08.002>
15. K. Zhuang, L. Cao, Y. Zheng et al., Studies on the molten salt reactor: code development and neutronics analysis of MSRE-type design. *J. Nucl. Sci. Technol.* **52**, 251–263 (2015). <https://doi.org/10.1080/00223131.2014.944240>
16. Y. Liu, L. Mei, X. Cai, Physics research for Molten Salt Reactor with different core boundaries. *Nucl. Tech.* **36**, 030601 (2013). **(in Chinese)**
17. A. Nuttin, D. Heue, A. Billebaud et al., Potential of thorium molten salt reactors: detailed calculations and concept evolution with a view to large scale energy production. *Progress Nucl. Energy* **46**, 77–99 (2005). <https://doi.org/10.1016/j.pnucene.2004.11.001>
18. Y. Liu, R. Guo, X. Cai et al., Breeding properties study on high-power thorium molten salt reactor. *ASME J. Nucl. Rad. Sci.* **5**, 011003 (2019). <https://doi.org/10.1115/1.4041272>
19. S. Yu, Y. Liu, P. Yang et al., Effect analysis of core structure changes on reactivity in molten salt experimental reactor. *Nucl. Tech.* **42**, 020603 (2019). <https://doi.org/10.11889/j.0253-3219.2019.hjs.42.020603>. **(in Chinese)**
20. W. Joe, J. Durkee, M.R. James et al., The MCNP6 delayed-particle feature. *Nucl. Technol.* **180**, 336–354 (2012). <https://doi.org/10.13182/NT12-22>
21. G. Zhu, Y. Zou, M. Li et al., Development of burn up calculation code for pebble-bed high temperature reactor at equilibrium state. *Atomic Energy Sci. Technol.* **5**, 890–896 (2015). <https://doi.org/10.7538/yzk.2015.49.05.0890>. **(in Chinese)**
22. Z. Xie, Physical analysis of nuclear reactors. Beijing: Atomic Energy Press, 139–160(2004). **(in Chinese)**
23. M.B. Chadwick, P. Obložinský, M. Herman et al., ENDF/B-VII.0: next generation evaluated nuclear data library for nuclear science and technology. *Nucl. Data Sheets* **107**, 29313060 (2017). <https://doi.org/10.1016/j.nds.2006.11.001>
24. J. Sun, Y. Zou, R. Yan et al., Study on the effect of core volume of PB-FHR on coolant temperature reactivity coefficient. *Nucl. Tech.* **37**, 120603 (2014). <https://doi.org/10.11889/j.0253-3219.2014.hjs.37.120603>. **(in Chinese)**
25. J. Sun, Y. Zou, R. Yan et al., Analysis of the coolant reactivity coefficients of FHRs with Li-6 contents of coolant. *Nucl. Tech.* **37**, 090605 (2014)